Title: **Magnetite pollution nanoparticles in the human brain**

Short title: Magnetite pollution particles in the human brain

Barbara A. Maher[1*], Imad A.M. Ahmed[2], Vassil Karloukovski[1], Donald A. MacLaren[3], Penny G. Foulds[4], David Allsop[4], David M.A. Mann[5], Ricardo Torres-Jardón[6], Lilian C. Calderon-Garciduenas[7,8]

[1*] Corresponding author, Centre for Environmental Magnetism and Palaeomagnetism, Lancaster Environment Centre, University of Lancaster, LA1 4YQ, U.K., b.maher@lancaster.ac.uk; (44)1524510268;[2] Department of Earth Sciences, University of Oxford, OX1 3AN, U.K.; [3] SUPA, School of Physics and Astronomy, University of Glasgow, G12 8QQ, U.K; [4] Division of Biomedical and Life Sciences, Faculty of Health and Medicine, University of Lancaster, LA1 4YQ, U.K.; [5]Centre for Clinical and Cognitive Neuroscience, Institute of Brain, Behaviour and Mental Health, University of Manchester, M6 8HD, U.K.; [6]Centro de Ciencias de la Atmósfera, Universidad Nacional Autónoma de México, Mexico City, 04310, México; [7]The University of Montana, Missoula, MT 59812, USA; [8]Universidad del Valle de México, Mexico City, 04850, México

Major classification: Physical Science

Minor classification: Environmental Science

Abstract

Biologically-formed nanoparticles of the strongly magnetic mineral, magnetite, were first detected in the human brain over 20 years ago (Kirschvink, J.L., Kobayashi-Kirschvink, A. & Woodford, B.J., 1992, Magnetite Biomineralization in the Human Brain. *P Natl Acad Sci USA* 89(16):7683-7687). Magnetite can have potentially large impacts on the brain due to its unique combination of redox activity, surface charge and strongly magnetic behaviour. We used magnetic analyses and electron microscopy to identify the abundant presence in the brain of magnetite nanoparticles that are consistent with high-temperature formation, suggesting therefore an external, not internal, source. Comprising a separate nanoparticle population from the euhedral particles ascribed to endogenous sources, these brain magnetites are often found with other transition metal nanoparticles, and they display rounded crystal morphologies and fused surface textures, reflecting crystallization upon cooling from an initially heated, iron-bearing source material. Such high-temperature magnetite 'nanospheres' are ubiquitous and abundant in airborne particulate matter (PM) pollution. They arise as combustion- derived, iron-rich particles, often associated with other transition metal particles, which condense and/or oxidise upon airborne release. Those magnetite pollutant particles which are < ~200 nm in diameter can enter the brain directly via the olfactory bulb. Their presence proves that externally sourced iron-bearing nanoparticles, rather than their soluble compounds, can be transported directly into the brain, where they may pose hazard to human health.

Keywords: brain magnetite, magnetite pollution particles, Alzheimer's disease, combustion-derived nanoparticles, airborne particulate matter

Significance Statement

We identify the abundant presence in the human brain of magnetite nanoparticles that match precisely the high-temperature magnetite 'nanospheres', formed by combustion and/or friction-derived heating, which are prolific in urban, airborne particulate matter (PM). Because many of the airborne magnetite pollution particles are < 200 nm in diameter, they can enter the brain directly

through the olfactory nerve, and by crossing the damaged olfactory unit. This discovery is important because nanoscale magnetite can respond to external magnetic fields, and is toxic to the brain, being implicated in production of damaging reactive oxygen species (ROS). Because enhanced ROS production is causally linked to neurodegenerative diseases such as Alzheimer's disease, exposure to such airborne PM-derived magnetite nanoparticles might need to be examined as a possible hazard to human health.

Introduction

Magnetic analyses of human brain samples have identified the presence of nanoparticles of magnetite, a strongly magnetic (ferrimagnetic) mixed Fe^{2+}/Fe^{3+} iron oxide(1-3). Based on their nano-scale dimensions and euhedral (cubo-octahedral or prismatic) crystal shapes, these magnetite nanoparticles are thought to have formed by biological processes(1, 4), via *in situ* crystallization, possibly within the 8 nm-diameter cores of the iron storage protein, ferritin (e.g. ref. (5)).

The specific presence of magnetite in the brain is important because it has been causally linked with potential cellular responses to external magnetic fields (e.g. in magnetic resonance imaging studies)(1), aging (6), and with neurodegenerative disease (e.g.(2, 3, 7)). Previous work has shown a correlation between the amount of brain magnetite and the incidence of Alzheimer's disease (AD)(2, 3). Neuropathological changes associated with AD include the formation of senile plaques, containing β-amyloid fibrils (e.g. (8, 9)). When associated with redox-active transition metal ions, such as Fe^{2+} ions, β-amyloid can generate damaging reactive oxygen species (ROS), directly contributing to oxidative brain damage, a key early feature of AD (e.g.(8-10)). Magnetite nanoparticles have been found directly associated with AD plaques and tangles (e.g. (11-13)). In vitro experimental data show that magnetite acts synergistically to enhance the toxicity of β-amyloid (7, 8).

We used magnetometry, high-resolution transmission electron microscopy (HRTEM), electron energy loss spectroscopy (EELS) and energy dispersive X-ray analysis (EDX) to examine

the mineralogy, morphology, and composition of magnetic nanoparticles in and from the frontal cortex of 37 human brain samples, obtained from subjects who lived in Mexico City(14) (29 cases; ages 3 to 85; 2 females) and in Manchester, U.K. (8 cases; ages 62 to 92; 5 females; Supporting Information Table 1). These brain magnetites display compelling similarity with the magnetite 'nanospheres' formed by combustion, which are ubiquitous and prolific in urban, airborne particulate matter (PM)(15-19). We report here identification of the presence in human brain tissue of magnetite nanoparticles with an external, rather than an endogenous, source.

Results

To quantify brain magnetic content, a cryogenic magnetometer was used to measure, at room and low temperature (77 K), the saturation magnetic remanence (SIRM) of frontal tissue samples, initially fresh-frozen and subsequently freeze-dried. The SIRM 77 K captures the magnetic contribution of ferrimagnetic grains which are so small (< ~20 nm) as to be magnetically unstable (superparamagnetic) at room temperature. The magnetic brain particles were then examined directly, by HRTEM and EDX analyses both of ultrathin tissue sections and of magnetically-extracted particles, after tissue digestion with the proteolytic enzyme, papain. Every analytical step was designed and monitored to preclude any possible magnetic contamination.

The brain magnetic analyses identify the presence in all of the samples of strongly magnetic, easily-magnetised nanoparticles, with concentrations ranging from 0.2 to 12 μg/g dry tissue (Fig. S1). The sample magnetic properties are dominated by behaviour characteristic of interacting clusters of ferrimagnetic magnetite or maghemite (Fig. S2). Although highest brain magnetite concentrations (>10 μg/g dry tissue) are seen in many of the oldest cases, several of the much younger Mexico City cases, some exposed to high ambient concentrations of fine-grained (< 2.5 μm aerodynamic diameter) airborne PM, also display high ferrimagnetic concentrations. Indeed, the highest brain magnetite content is found in a 32-year old, Mexico City resident (Fig. S1).

HRTEM and EELS analyses of the tissue sections identify the presence within frontal cells of magnetite, occurring as two distinct types of nanoparticle (Fig. 1 and Figs. S3 and S4). The majority of particles display rounded, even spherical morphologies (Fig. 1a, with higher magnification in

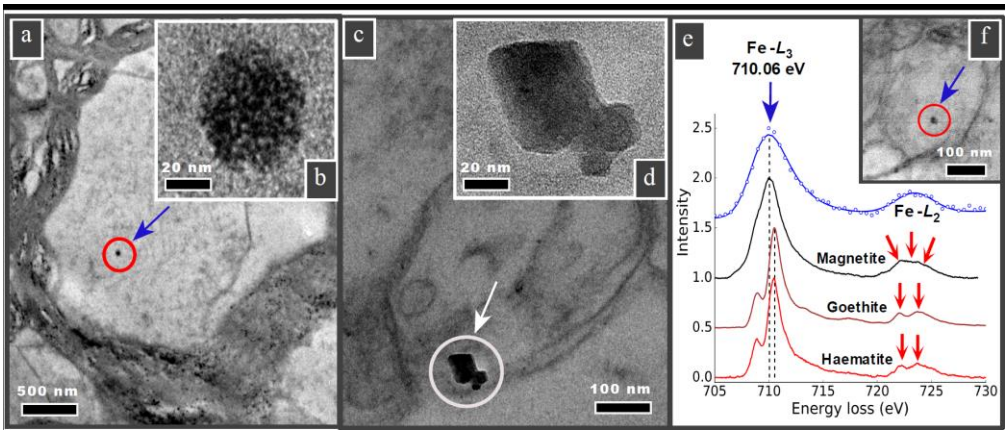

Fig. 1. Transmission electron micrographs of brain thin sections, identifying two distinct types of magnetite morphologies within frontal cells: (a and f) rounded particles (a shown at higher magnification in b); and (c) angular, euhedral particles, which we attribute to endogenous formation (particles in c shown at higher magnification in d). e): EELS spectra (in blue) for the rounded particle shown in (f) and for standard iron oxide species. The position of the Fe-L_3 edge absorption peak, the broad feature of the Fe-L_2 (compared with the sharp edges, arrowed, of the fully-oxidised Fe^{3+} phases), and the integrated areas of the L_3/L_2 (5.5) and the Fe/O (0.56) are all consistent with magnetite (also see Figs. S3 and S4).

Fig. 1b; and Fig. 1f), with diameters between 10 and 150 nm (Fig. S5). The additional presence in the brain cells of other transition metal nanoparticles, containing Pt, Ni, Co (and possibly Cu), is identified by EELS (Fig. S6) and EDX (Figs. S7 and S8). These rounded magnetites contrast strongly with the angular, cubo-octahedral magnetite crystals also observed (relatively very rarely) within the brain tissue samples (Fig. 1c, and with higher magnification in Fig. 1d).

Crystallographic analysis of the particles within the tissue sections is difficult (due to rapid carbon build-up under the microscope electron beam). We therefore examined magnetically-

extracted (20) brain particles, in order to more fully characterize their mineralogy, surface textures and particle size distribution. In accord with the observations on the untreated tissue samples, many of the extracted particles display rounded to spherical morphologies (Fig. 2, and Figs. S7-S10).

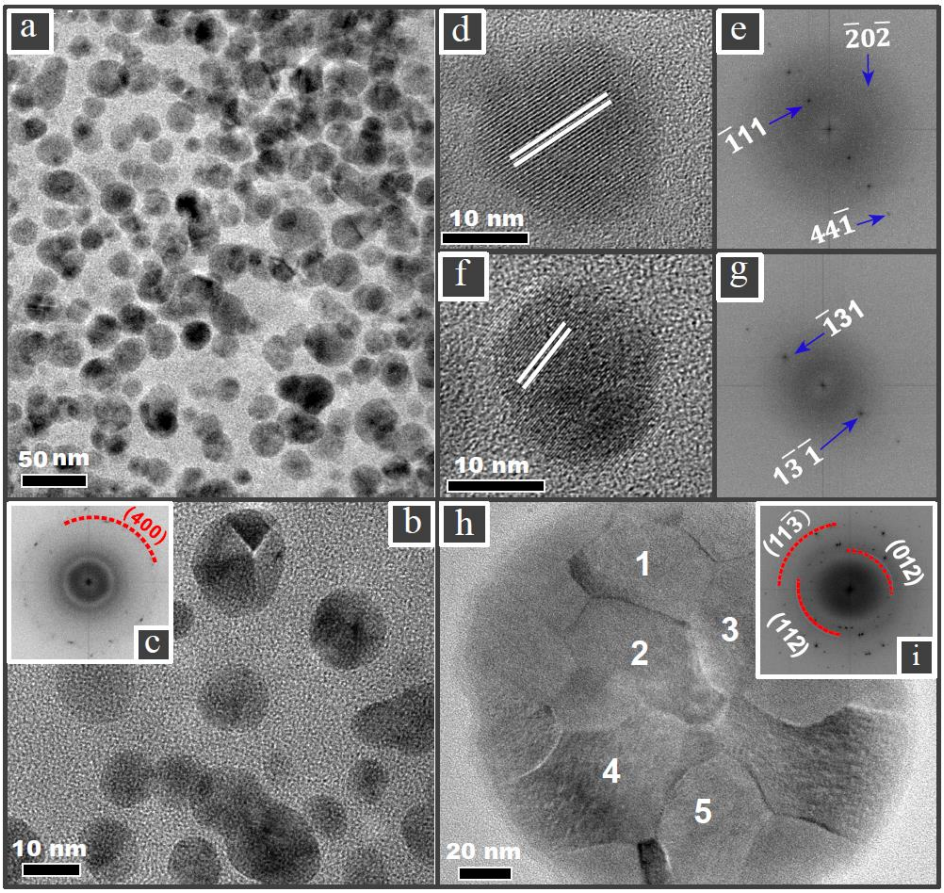

Fig. 2. Transmission electron micrographs of rounded particles magnetically extracted from human brain samples: (a,d,f and h) Mexico City cases; b) Manchester case. (h) A large (~150-nm diameter) spherical particle with fused, interlocking magnetite/ maghemite surface crystallites. (c, e and g): Indexing of the lattice fringes of the brain particles is consistent with the (400) reflection of magnetite and (i) mixed magnetite and maghemite of selected areas 1-5 in (h).

In particular, some have fused surface crystallites (Fig. 2 h) that would be very difficult to reconcile with low-temperature growth or dissolution formation processes. Indexing of the lattice fringes of the HRTEM of these particles is consistent with the magnetite crystal structure (Fig. 2c, e, g). Some

surface oxidation towards its oxidized counterpart, maghemite, is evident (Fig. 2i). The particle size distribution of the rounded brain magnetite particles is notably broad, with a median (longest) diameter of 18 nm, and maximum diameter of ~150 nm (Fig. S5). Such dimensions greatly exceed those of nanoparticles formed within the 8-nm diameter of ferritin cores(5).

Discussion

The geometric, angular particles (comprising ~1 in 500 magnetite NPs in our samples) resemble the *in situ*, biogenic magnetite previously reported (1, 4); we thus ascribe these euhedral magnetite particles to endogenous formation. The abundant, rounded magnetite nanoparticles (up to ~150-nm diameter, with distinctive surface textures, and co-occurring with other PM-associated metals, including Pt), have not been identified previously in brain tissue sections. Apparently similar spherical structures, with diameters of 8 to 50 nm, have been found recently within amyloid plaque cores isolated from human brain (13), but were attributed to a biological rather than an external pollution-derived source. However, the surface textures, size and size distribution of the spherical magnetites identified in our study, and the co-occurrence of PM-associated transition metal nanoparticles, are all inconsistent with the characteristics of biogenically-formed magnetite (1, 4, 12). They bear compelling resemblance, instead, to the rounded/spherical magnetite nanoparticles (nanospheres) which are both ubiquitous and prolific within airborne, high-temperature (combustion-derived) PM (15-19, 21). The rounded shapes of these airborne, PM-derived magnetites (Fig. 3, and Fig. S11), and fusing of interlocking, surface crystallites (Fig. 3c and d), reflect their high-temperature sources, and their subsequent crystallization, upon rapid cooling and/or oxidation, as Fe-rich nanospheres. Depending on PM source/s (vehicular, subway, industrial, indoor), other transition metals are often co-associated with magnetite and other pollution nanoparticles (15-17, 19). Pt release, for instance, is associated with increasing vehicular use of catalytic converters (e.g. (22)). Frictional heating, e.g. of brake pads, can also produce high-temperature magnetite nanoparticles (21). Magnetite can arise from combustion of many types of organic matter, depending on heating

temperature and atmosphere, and source Fe content (23-25).

Although PM mass has conventionally been used for setting of legislative airborne PM concentration limits, it is possible that ultrafine particle size and number are of greater significance in

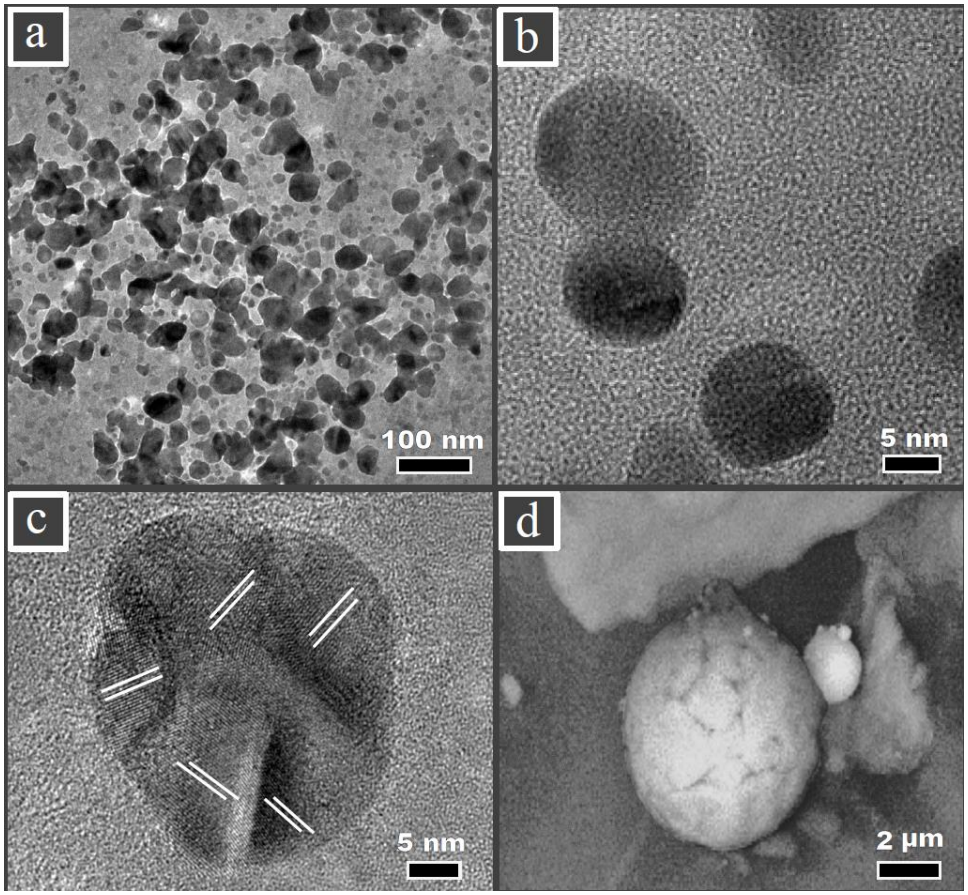

Fig. 3. TEM/SEM micrographs of anthropogenic (combustion-derived), magnetically-extracted airborne particles: a) and b): magnetite nanoparticles from airborne PM (< 10 µm), from Cable Street, Lancaster, U.K. (March 2009), sampled with a cascade impactor. Many particles display rounded profiles; some are fused together; c) and d) spherical magnetite particles, Didcot power station, comprising fused magnetite particles (note the variable lattice orientations in (c) and the fused surface crystallites in (d)).

terms of mortality (26) and health impacts (e.g.(27)). Our magnetic measurements of roadside airborne PM [in Lancaster, U.K. (28)] indicate magnetite particle numbers equivalent to ~ 2.01 x 10^8

m^{-3} of roadside air, for ~50 nm-sized magnetite particles, for an ambient PM_{10} concentration of ~40 μg m^{-3} (compared, for example, with the annual mean PM_{10} for Mexico City of between ~ 30 and 70 μgm^{-3}).

The abundant combustion-derived magnetite particles found in airborne PM can range widely in size, from less than 5 nm to more than 1 μm (15-17, 19). Those particles of nanoscale dimensions, requiring analysis by transmission rather than scanning electron microscopy, have, until recently, received less attention than the larger, often more heterogenous spherules. Magnetite nanospheres up to $\lesssim$ 200 nm can have a direct entry route to the brain through the axons of the olfactory nerve, as suggested by experimental studies on carbon (29) and TiO_2 nanoparticles (30), and the reported presence of nanoparticles in the olfactory bulb of some Mexico City cases (14, 31-33).

Although many of the highly magnetic brain samples come from the older Manchester cases (> 65 years at death), especially those with severe to moderate AD, equivalent or higher magnetite concentrations are also displayed by young (< 40 years at death) Mexico City residents, especially those exposed to high $PM_{2.5}$ levels (annual mean $\gtrsim$ 25 μg m^{-3}). Increased metals content and AD neuropathological hallmarks have been found in young human brains exposed to high airborne $PM_{2.5}$ concentrations in Mexico City (14, 33). However, it was not previously known if the presence of metals in AD brains was due to transport to the brain of nanoparticles themselves or of their solubilized compounds. Our HRTEM results provide compelling evidence for the presence of externally sourced magnetite, and other metal-bearing, nanoparticles in the frontal cortex of both the Mexican City and Manchester cases. It is notable that less than 5% of AD cases are directly inherited, indicating that non-genetic (environmental) factors, and/or gene/environment interactions, are likely playing a major role in initiating and/or promoting the disease. Jung et al.(34) found a 138% risk of increase of AD per increase of 4.34 μg m^{-3} in $PM_{2.5}$ over a 9-year follow-up period in 95,690 individuals in Taiwan. It is not yet understood which PM properties (e.g. size, number, mineralogy and associated chemical species) contribute most to toxic effects (e.g. (35)). Our preliminary magnetic results regarding both PM exposure and AD are thus both intriguing and

warrant more intensive study. Because of their combination of ultrafine size, specific brain toxicity, and ubiquity within airborne PM, pollution-derived magnetite nanoparticles might require consideration as a possible AD risk factor. In addition to occupational settings (including, for example, exposure to printer toner powders (36)), higher concentrations of magnetite pollution nanoparticles are likely to arise in the indoor environment from open fires (24) or poorly-sealed stoves used for cooking and/or heating, and in the outdoor environment from vehicle (especially diesel) and/or industrial PM sources.

Materials and Methods

Brain samples. Fresh, frozen brain tissues were obtained from 38 individuals (Table S1); 9 from the Manchester Brain Bank (ethical review and approval by the Manchester Brain Bank Management Committee and the Newcastle and North Tyneside 1 Regional Ethics Committee), 29 from Mexico City, from forensic cases (fatal accidents) with no identifiable personal data, not meeting the regulatory definition of human subject research (University of Montana Institutional Review Board). A block (~25 g) of tissue was cut from the frontal lobes; sub-samples were cut using non-magnetic (PTFE) instruments. The Manchester samples were dissected into grey (9 samples) and white matter (8 samples).

To preclude any contamination, or operator bias, samples were handled with non-magnetic instruments in a laminar flow clean bench environment, measured blind to diagnostics, and sample holder remanences removed. The tissue samples were freeze-dried and placed in polystyrene sample holders (10 cc) for magnetic measurements.

Magnetic analyses. Magnetic measurements were made at the Centre for Environmental Magnetism and Palaeomagnetism, Lancaster University, using superconducting quantum interference device (SQUID) magnetometry. RT isothermal remanent magnetization (IRMs) (Fig. S2a) were measured with a GM400 Cryogenic Magnetometer (Cryogenic Consultants Ltd.; mean background noise level

5.9 x10^{-11} Am^2); Low-temperature IRMs (Fig. S2b) were measured at temperatures between 293 and 77 K (± 0.5 K) on a single axis MPMS XL magnetometer (Quantum Design). To identify magnetic grain sizes and/or magnetic interactions (37), anhysteretic remanence (ARM) was induced in a decaying (100 mT, peak) alternating magnetic field (af), with a small superimposed DC field (0.08 mT), and subsequently af-demagnetised (Fig. S2c). Stepwise remanence acquisition was measured with incremental application of DC fields of 10, 20, 30, 50, 75, 100, 300 mT and 1T. The samples were cooled to 77 K, subjected to an applied DC field, 1 T, and their remanence measured as they warmed to room temperature.

Tissue sections

Magnetically-extracted particles. A subset of samples (6 tissue samples, and 1 blank without any tissue) was subjected to a magnetic extraction procedure, designed to maximize removal of sub-micrometre ferrimagnets (20). All reagents were prepared from ultra-purity MilliQ-water and pre-filtered (< 0.1 µm PTFE membrane filter) to preclude any particulate contamination; all instruments and sample holders were non-magnetic (PTFE and polystyrene, respectively).

Papain from papaya latex (twice-crystallized, Sigma) was solubilized in 50 mM sodium acetate (pre-filtered and magnetically measured multiple times to demonstrably preclude magnetic contamination). The tissue samples were digested overnight in papain at 65 °C and at fixed pH 7.0±0.02, in a strictly oxygen-free environment inside a particulate-clean lab. The resultant suspension was circulated continuously (2-3 days, with a peristaltic pump) past a magnetised probe, producing a high field gradient at its tip (maximum field ~40 mT). The magnetically-extracted particles were mounted on holey carbon films on carbon-coated copper grids for TEM.

HRTEM, EELS and EDX. Electron microscopy was conducted on two instruments, a JEOL ARM200cF and an FEI Tecnai F20, operated at 200kV. A Gatan Quantum spectrometer was used for EELS in scanning TEM mode. Due to rapid carbon build-up under the electron beam, only point acquisition spectra were collected; each spectrum typically summed from several spectra from each nanoparticle and from multiple nanoparticles. This procedure also minimised the electron dose

experienced by individual nanoparticles and ensured that their chemical reduction was avoided. Time-dependent observations did not reveal any obvious structural or spectroscopic changes to the nanoparticles within the acquisition time (but were observed under prolonged exposure) and we conclude that the EELS data presented are representative of the nanoparticles' as-formed chemistry. EELS data were processed in python using Hyperspy package. To determine dominant lattice spacings, Fast Fourier Transforms (FFT) of high resolution micrographs were compared to a simulated diffraction pattern of face-centered cubic magnetite (space group $Fd\bar{3}m$, No. 227, a = 8.3941 Å), and maghemite (space group $P4_332$, No. 212, a = 8.3457 Å). Sample sensitivity under STEM imaging precluded elemental mapping by EDX.

Acknowledgements

We appreciate the reviewers' comments which improved our manuscript. We thank the University of Leeds EPSRC Nanoscience and Nanotechnology Facility (LENNF) for access to the HRTEM and Dr Zabeada Aslam for her technical help, Dr Mark Taylor (Lancaster University) for assistance with tissue sub-sampling, and Angélica González-Maciel, Instituto Nacional de Pediatria, CDMX, for assistance with electron-microscopy sub-sampling. We acknowledge the support of the Manchester Brain Bank by Alzheimer's Research UK and Alzheimer's Society through their funding of Brains for Dementia Research (BDR) initiative, and service support costs from Medical Research Council.

Author contributions

BAM designed research; BAM, IAMA, VK and DAM performed research; DA and PF contributed new reagents/analytic tools; BAM, IAMA, VK, DAM, DMAM, RT-J and LC-G analysed data; BAM wrote the paper; DMAM provided brain tissue samples and medical diagnosis data; RT-J provided airborne $PM_{2.5}$ data for the Mexico City cases; and LCG provided brain tissue samples.

References

1. Kirschvink JL, Kobayashikirschvink A, & Woodford BJ (1992) Magnetite Biomineralization in the Human Brain. *P Natl Acad Sci USA* 89(16):7683-7687.
2. Pankhurst Q, Hautot D, Khan N, & Dobson J (2008) Increased levels of magnetic iron compounds in Alzheimer's disease. *Journal of Alzheimer's Disease* 13(1):49-52.
3. Hautot D, Pankhurst Q, Khan N, & Dobson J (2003) Preliminary evaluation of nanoscale biogenic magnetite in Alzheimer's disease brain tissue. *Proceedings of the Royal Society of London B: Biological Sciences* 270(Suppl 1):S62-S64.
4. Schultheiss-Grassi PP, Wessiken R, & Dobson J (1999) TEM investigations of biogenic magnetite extracted from the human hippocampus. *Biochimica et Biophysica Acta (BBA)-General Subjects* 1426(1):212-216.
5. Quintana C, Cowley JM, & Marhic C (2004) Electron nanodiffraction and high-resolution electron microscopy studies of the structure and composition of physiological and pathological ferritin. *Journal of structural biology* 147(2):166-178.
6. Dobson J (2002) Investigation of age-related variations in biogenic magnetite levels in the human hippocampus. *Experimental brain research* 144(1):122-126.
7. Teller S, Tahirbegi IB, Mir M, Samitier J, & Soriano J (2015) Magnetite-Amyloid-beta deteriorates activity and functional organization in an in vitro model for Alzheimer's disease. *Sci Rep-Uk* 5.
8. Allsop D, Mayes J, Moore S, Masad A, & Tabner BJ (2008) Metal-dependent generation of reactive oxygen species from amyloid proteins implicated in neurodegenerative disease. *Biochemical Society Transactions* 36(6):1293-1298.
9. Tabner BJ, Mayes J, & Allsop D (2010) Hypothesis: soluble Aβ oligomers in association with redox-active metal ions are the optimal generators of reactive oxygen species in Alzheimer's disease. *International Journal of Alzheimer's Disease* 2011.
10. Castellani RJ, *et al.* (2007) Iron: the Redox-active center of oxidative stress in Alzheimer disease. *Neurochemical research* 32(10):1640-1645.
11. Collingwood J & Dobson J (2006) Mapping and characterization of iron compounds in Alzheimer's tissue. *Journal of Alzheimer's Disease* 10(2, 3):215-222.
12. Quintana C, *et al.* (2006) Study of the localization of iron, ferritin, and hemosiderin in Alzheimer's disease hippocampus by analytical microscopy at the subcellular level. *Journal of structural biology* 153(1):42-54.
13. Plascencia-Villa G, *et al.* (2016) High-resolution analytical imaging and electron holography of magnetite particles in amyloid cores of Alzheimer's disease. *Sci Rep-Uk* 6.
14. Calderón-Garcidueñas L, *et al.* (2016) Prefrontal white matter pathology in air pollution exposed Mexico City young urbanites and their potential impact on neurovascular unit dysfunction and the development of Alzheimer's disease. *Environmental research* 146:404-417.
15. Mitchell R & Maher BA (2009) Evaluation and application of biomagnetic monitoring of traffic-derived particulate pollution. *Atmospheric Environment* 43(13):2095-2103.
16. Moreno T, *et al.* (2015) A new look at inhalable metalliferous airborne particles on rail subway platforms. *Science of The Total Environment* 505:367-375.
17. Chen Y, Shah N, Huggins FE, & Huffman GP (2006) Microanalysis of ambient particles from Lexington, KY, by electron microscopy. *Atmospheric Environment* 40(4):651-663.
18. Puffer JH, Russell EWB, & Rampino MR (1980) Distribution and Origin of Magnetite Spherules in Air, Waters, and Sediments of the Greater New-York-City Area and the North-Atlantic Ocean. *J Sediment Petrol* 50(1):247-256.
19. Liati A, Pandurangi SS, Boulouchos K, Schreiber D, & Dasilva YAR (2015) Metal nanoparticles in diesel exhaust derived by in-cylinder melting of detached engine fragments. *Atmospheric Environment* 101:34-40.
20. Hounslow MW & Maher BA (1996) Quantitative extraction and analysis of carriers of magnetization in sediments. *Geophysical Journal International* 124(1):57-74.
21. Kukutschova J, *et al.* (2011) On airborne nano/micro-sized wear particles released from low-metallic automotive brakes. *Environ Pollut* 159(4):998-1006.
22. Gomez B, Gomez M, Sanchez J, Fernandez R, & Palacios M (2001) Platinum and rhodium distribution in airborne particulate matter and road dust. *Science of The Total Environment* 269(1):131-144.
23. Jordanova N, *et al.* (2006) Magnetism of cigarette ashes. *J Magn Magn Mater* 301(1):50-66.
24. Mcclean RG & Kean WF (1993) Contributions of Wood Ash Magnetism to Archaeomagnetic Properties of Fire Pits and Hearths. *Earth Planet Sc Lett* 119(3):387-394.
25. Abdul-Razzaq W & Gautam M (2001) Discovery of magnetite in the exhausted material from a diesel engine. *Appl Phys Lett* 78(14):2018-2019.
26. Brunekreef B & Forsberg B (2005) Epidemiological evidence of effects of coarse airborne particles on health. *European Respiratory Journal* 26(2):309-318.
27. Pieters N, *et al.* (2015) Blood pressure and same-day exposure to air pollution at school: associations with nano-sized to coarse PM in children. *Environmental health perspectives* 123(7):737.
28. Halsall CJ, Maher BA, Karloukovski VV, Shah P, & Watkins SJ (2008) A novel approach to investigating indoor/outdoor pollution links: Combined magnetic and PAH measurements. *Atmospheric Environment* 42(39):8902-8909.

29. Oberdörster G, *et al.* (2004) Translocation of inhaled ultrafine particles to the brain. *Inhalation toxicology* 16(6-7):437-445.
30. Wang J, *et al.* (2008) Time-dependent translocation and potential impairment on central nervous system by intranasally instilled TiO 2 nanoparticles. *Toxicology* 254(1):82-90.
31. Calderon-Garciduenas L, *et al.* (2003) DNA damage in nasal and brain tissues of canines exposed to air pollutants is associated with evidence of chronic brain inflammation and neurodegeneration. *Toxicologic pathology* 31(5):524-538.
32. Block ML & Calderón-Garcidueñas L (2009) Air pollution: mechanisms of neuroinflammation and CNS disease. *Trends in neurosciences* 32(9):506-516.
33. Calderón-Garcidueñas L, *et al.* (2013) The impact of environmental metals in young urbanites' brains. *Experimental and Toxicologic Pathology* 65(5):503-511.
34. Jung C-R, Lin Y-T, & Hwang B-F (2015) Ozone, particulate matter, and newly diagnosed Alzheimer's disease: a population-based cohort study in taiwan. *Journal of Alzheimer's Disease* 44(2):573-584.
35. Könczöl M, *et al.* (2011) Cytotoxicity and genotoxicity of size-fractionated iron oxide (magnetite) in A549 human lung epithelial cells: role of ROS, JNK, and NF-κB. *Chemical Research in Toxycology* 24(9):1460-1475.
36. Gminski R, *et al.* (2011) Genotoxic effects of three selected black toner powders and their dimethyl sulfoxide extracts in cultured human epithelial A549 lung cells in vitro. *Environmental and molecular mutagenesis* 52(4):296-309.
37. Maher BA (1988) Magnetic-Properties of Some Synthetic Sub-Micron Magnetites. *Geophys J Int* 94(1):83-96.

Figure Legends

Fig. 1. Transmission electron micrographs of brain thin sections, identifying two distinct types of magnetite morphologies within frontal cells: rounded particles, shown in a), and at higher magnification in b), and f); and angular, euhedral particles, which we attribute to endogenous formation, shown in c) and at higher magnification in d). e): EELS spectra (in blue) for the rounded particle shown in f) and for standard iron oxide species. The position of the Fe-L_3 edge, the broad feature of the Fe-L_2 (compared with the sharp edges, arrowed, of the fully-oxidised Fe^{3+} phases), and the integrated areas of the L_3/L_2 (5.5) and the Fe/O (0.56) are all consistent with magnetite (and see Supporting Information Figs. 6 and 9).

Fig. 2. Transmission electron micrographs of rounded particles magnetically extracted from human brain samples: a) Mexico City case; b) Manchester case; d, f and h) Mexico City cases, h) showing a large (~150 nm diameter) spherical particle with fused, interlocking magnetite/ maghemite surface crystallites. Insets: indexing of the lattice fringes of the brain particles is consistent with the (400) reflection of magnetite (c, e, g) and mixed magnetite and maghemite of selected areas (1-5) in h).

Fig. 3. TEM/SEM micrographs of anthropogenic (combustion-derived), magnetically-extracted airborne particles: a) and b): magnetite nanoparticles from airborne PM (< 10 μm), from Cable

Street, Lancaster, U.K. (March 2009), sampled with a cascade impactor. Many particles display rounded profiles; some are fused together; c) and d) spherical magnetite particles, Didcot power station, comprising fused magnetite particles (note the variable lattice orientations in (c) and the fused surface crystallites in (d)).